Published in final edited form as:
Epilepsy Behav. 2013 May ; 27(2): 319–325. doi:10.1016/j.yebeh.2013.02.018.

Brain MR Spectroscopic Abnormalities in "MRI-negative" Tuberous Sclerosis Complex Patients

William E. Wu[1], **Ivan I. Kirov**[1], **Assaf Tal**[1], **James S. Babb**[1], **Sarah Milla**[1], **Joseph Oved**[2,3], **Howard L. Weiner**[2,3], **Orrin Devinsky**[3,4,5], and **Oded Gonen**[1]

[1]Department of Radiology, New York University School of Medicine, New York, NY 10016, USA

[2]Department of Pediatrics, New York University School of Medicine, New York, NY 10016, USA

[3]Department of Neurosurgery, New York University School of Medicine, New York, NY 10016, USA

[4]Department of Neurology, New York University School of Medicine, New York, NY 10016, USA

[5]Department of Psychiatry, New York University School of Medicine, New York, NY 10016, USA

Abstract

Since approximately 5–10% of the ~50,000 Tuberous Sclerosis Complex (TSC) patients in the US are "MRI-negative," our goal was to test the hypothesis that they nevertheless exhibit metabolic abnormalities. To test this, we used proton-MR spectroscopy to obtain and compare gray and white matter (GM, WM) levels of the neuronal marker *N*-acetylaspartate (NAA); the glial marker, *myo*-inositol (*m*I) and its associated creatine (Cr) and choline (Cho), between two "MRI-negative" female TSC patients (5- and 43-year-olds) and their matched controls. The NAA, Cr, Cho and *m*I concentrations in the pediatric control: 9.8, 6.3, 1.4 and 5.7 millimolar, were similar to the patient's; whereas the adult patient revealed a 17% WM NAA decrease and 16% WM Cho increase from their published means for healthy adults - both outside their respective 90% prediction intervals. These findings suggest that longer disease duration and/or *TSC2* gene mutation may cause axonal dysfunction and demyelination.

Keywords

Adult, Brain Diseases; Magnetic Resonance Imaging; Magnetic Resonance Spectroscopy; Neurology; Pediatric; Tuberous Sclerosis

INTRODUCTION

Tuberous sclerosis complex (TSC), a neurocutaneous disorder affecting ~1:6000 live births, affects ~50,000 in the US (1). In 85% of cases, the disorder results from mutations in the *TSC1* (9q34) or *TSC2* (16p13·3) genes that code for hamartin and tuberin, respectively. The latter are more common and cause more severe pathology (2 disease in multiple organs).

Corresponding Author: Oded Gonen, PhD, Department of Radiology, New York University School of Medicine, 660 First Avenue, 4th Floor, New York, New York 10016, Telephone/FAX: (212) 263-3532/(212) 263-7541, oded.gonen@med.nyu.edu.

Clinical symptoms and pathological findings in TSC are primarily from mammalian target of rapamycin complex 1 (mTORC1) hyperactivity. TSC affects multiple organ systems prominently involving the brain, skin, kidneys and lungs (3, 4). Neurological disorders are probably the leading cause of morbidity and mortality (5) - seizures affect up to 90% of patients, often with early onset and medical intractability, and are associated with high rates of intellectual disability and autism (6–9). Other neuropsychiatric disorders complicate TSC: language delays, impaired social and emotional skills, aggressive behavior, attention-deficit, anxiety, and affective and motor disorders (9, 10).

TSC brain lesions include subependymal giant cell astrocytomas (SEGAs) and nodules that can occur throughout the brain [although predominate in subcortical nuclei (11)], cortical and subcortical tubers, cerebral cortex and cerebellum developmental malformations comprised of disorganized structures lacking six-layered lamination and containing dysplastic neurons, astrocytes and/or giant cells. The tubers' number and size correlate in some studies with autism, intellectual disability and epilepsy severity (12, 13). In patients with refractory epilepsy and a single large tuber, its resection is associated with more than 90% reduction in seizures (14). The relation between MRI lesion burden and neurologic phenotype, however, is imperfect: TSC patients with many tubers can have normal IQ, while others with just a few may suffer severe intellectual disability (13). Moreover, some TSC patients with clinically symptomatic SEGAs have many cortical tubers but no seizures, and require no anti-epileptic medication. Finally, TSC animal models have been able to replicate hyper-excitable brains and seizures, but lack tubers (15–17).

Fluid-attenuated inversion recovery (FLAIR) MRI is the most sensitive sequence to identify the tubers, with a false-negative rate of ‹0.5% versus 21% for T_2-weighted MRI (18). This is due to the long T_2 weighting and cerebrospinal fluid (CSF) signal suppression that enhances the sensitivity to small subcortical and gyral core (enlarged gyri with central hyperintensity) tubers, although in neonates and infants, MRI signal intensity changes may be opposite to those of older children or adults (19). Despite FLAIR's high sensitivity, only 90–95% of TSC patients exhibit brain tubers on MRI (18, 19). The remaining show none despite neuropsychiatric symptoms (18). In these patients, mTORC1 pathway hyperactivation--the underlying pathogenic mechanism of TSC--may interfere with cortical development and contribute to functional impairments by producing giant cells, dysplastic neurons and other MRI-occult microscopic changes (20, 21).

Aberrant neuronal and glial function in TSC may be monitored non-invasively through their proton-MR spectroscopy (^{1}H-MRS)-observed markers: *N*-acetylaspartate (NAA) for neurons (22); *myo*-inositol (*m*I) for the astroglia (23, 24), creatine (Cr) and choline (Cho) that are more abundant in the latter (25). Our goal, therefore, was to test whether "MRI-negative" TSC patients exhibit: *(a)* increases in the astroglial metabolites: *m*I, Cr and Cho; and *(b)* NAA levels similar to controls', since mTORC1 processes produce dysfunctional neurons but do not damage existing ones. Towards these ends and since TSC pathology is diffuse, we applied three-dimensional (3D) ^{1}H-MRS to the brains of two MRI-negative TSC patients and their healthy matched controls.

MATERIALS AND METHODS

Human Subjects

Two female TSC patients, a 5- and 43-year old, and their age- and gender-matched controls were prospectively enrolled. The 5-year old patient did not have either *TSC1* or *2* mutation although she met criteria for "clinically-definite" TSC (26) and was diagnosed with cardiac rhabdomyomas at birth. Seizures began at age 2 years and she developed medically refractory partial (simple and partial complex, secondary generalized) and symptomatic

generalized (myoclonic, atypical absence, and tonic) seizures. Electroencephalogram showed generalized spike-wave and left occipital discharges. Her examination revealed five hypopigmented macules, global developmental delay and gait ataxia. Bilateral subdural strip studies revealed multifocal and diffuse seizure onsets that were inoperable. The 43-year old woman was diagnosed with a *TSC2* gene mutation, facial angiofibromas and renal angiomyolipomas, but had no history of neurological symptoms. Both patients and controls had unremarkable brain MRI. The children's parents and the adults gave written Institutional Review Board-approved informed consent.

MR Acquisition

Measurements on pediatric subjects were done in a 1.5 T MRI scanner with its standard transmit-receive circularly-polarized head-coil (AVANTO®, Siemens AG, Erlangen Germany). Axial T_2-weighted turbo-spin echo (TSE; *TE*/*TR*=107/4770 ms) MRI were acquired at 220×220 mm^2 field-of-view (FOV), 256×256 matrix, 5.0 mm slice thickness. Measurements on the adults were done in a 3 T MRI scanner (TRIO®, Siemens AG, Erlangen, Germany) with a transmit-receive circularly-polarized head-coil (TEM3000, MRinstruments, Minneapolis, MN). The TSE MRI were acquired at 256×256 mm^2 FOV, 512×512 matrix, 3.7 mm slice thickness.

In the children, following our chemical-shift imaging (CSI) based autoshim procedure (27), and depending on brain size, a 9 – 10 cm anterior-posterior (AP) by 7 – 8 cm left-right (LR) by 4 cm inferior-superior (IS) =252 – 320 cm^3 ^{1}H-MRS volume-of-interest (VOI) was centered on the corpus callosum, as shown in Fig. 1. It was excited with *TE*/*TR*=30/1360 ms PRESS and partitioned using Hadamard spectroscopic imaging into four axial slices, each encoded with 16×16 2D-CSI over a 16×16 cm^2 (LR×AP) FOV (28). The VOI was defined in these slices' planes with two 8 ms numerically optimized 180° pulses (6.3 kHz bandwidth) to yield 252 – 320 voxels, each1.0 cm^3. The MRS signal was acquired for 512 ms at ±0.5 kHz bandwidth. At three averages the ^{1}H-MRS took 35 minutes and the protocol was ¾ hour.

In the two adults, a 10×8×4.5 cm^3=360 cm^3 (AP×LR×IS) ^{1}H-MRS VOI was used, as shown in Fig. 2 and excited with *TE*/*TR*=35/1800 ms PRESS. It was partitioned into six axial slices with three second-order Hadamard encoded slabs (28). These were encoded with 16×16 2D-CSI over a 16×16 cm^2 (LR×AP) FOV and the VOI was defined in slices' planes by two 11.2 ms optimized 180° pulses (4.5 kHz bandwidth) yielding 8×10×6=480 voxels, 0.75 cm^3 each. The ^{1}H-MRS signal was acquired for 256 ms at ±1 kHz bandwidth; at two averages, it took 31 minutes.

Metabolite Quantification

Processing was done with in-house software that removed the residual water signal in the time domain, zero-filled the data from 512 to 2048 points, voxel-shifted to align the CSI grid with the NAA VOI and Fourier transformed in the time, AP and LR and Hadamard reconstructed along the IS directions. The spectra were frequency-aligned and phased in reference to the NAA peak in each voxel (29); and the relative level of the i^{th}=NAA, Cr, Cho or *m*I in each voxel estimated from its peak area, S_i, using prior knowledge modeling software (30). These were scaled into absolute concentrations, C_i, relative to their signals from a 2 L reference sphere of C_i^{vitro}=12.5, 10.0, 3.0 and 7.5 mM NAA, Cr, Cho and *m*I in water at physiological ionic strength:

$$C_i = C_i^{vitro} \cdot \frac{S_i}{S_R} \cdot \left(\frac{P^{180°}}{P_R^{180°}}\right)^{1/2} \cdot \frac{1}{\mathrm{T_f}}, \quad [1]$$

where S_R is the reference metabolites' signal and T_f the VOI tissue fraction, $P^{180°}$ and $P_R^{180°}$ the radio-frequency power for a non-selective 1 ms 180° pulse on subject and reference and f_i-s correct for different relaxation times *in vivo* (T_1^{vivo}, T_2^{vivo}) and in the reference (T_1^{vitro}, T_2^{vitro}):

$$f=\frac{\exp(-TE/T_2^{vitro})}{\exp(-TE/T_2^{vivo})}\cdot\frac{1-\exp(-TR/T_1^{vitro})}{1-\exp(-TR/T_1^{vivo})}. \quad [2]$$

We used the reported 3 T T_1^{vivo} values of 1360, 1300, 1145 and 1170 ms for NAA, Cr, Cho and *m*I (31) and T_2^{vivo} of 350, 174, 251 and 200 ms (32, 33). The 1.5 T metabolite T_2^{vivo} values used were 357, 216, 332 and 200 ms (34). Since the corresponding T_1^{vivo}s are reported to not significantly differ from 3 T (34), the same values were used at both fields.

The global concentration of the *i*-th metabolite in the VOI of a subject, C_i, was obtained by summing all the spectra in the VOI. This strategy is appropriate for diffuse disorders, retains the individual (narrow) spectra linewidth and dramatically improves the signal-to-noise-ratio (SNR), *i.e.,* the precision (35), by the square root of the number of voxels, ≈20 fold in this study (36):

$$C_i=\frac{\sum_{j=1}^{n}Q_{ij}}{\sum_{j=1}^{n}\left(V_j^{GM}+V_j^{WM}\right)}\cdot f_i \text{mM/g wet weight}, \quad [3]$$

where n is the number of voxels in the VOI and f_i is given by Eq. [2] for the *i*-th metabolite.

Brain Volumetry

The TSE images were segmented with our FireVoxel package that also works well on pediatric brains, as shown in Fig. 3 (37). It first corrects the images for non-uniform intensities due to the coil's RF inhomogeneity, using the common histogram devolution method of Sled *et al.* (38). Next, a WM signal intensity, I_{WM}, is selected in a periventricular seed region. Following automatic detection of all pixels at or above 50% (but below 192.5% to exclude the CSF) of I_{WM}, every slice's tissue-mask is constructed in three steps: morphological erosion; recursive region growth retaining pixels connected to the seed; and morphological inflation to reverse the erosion effect. Pixels of intensity above 192.5% of I_{WM} are classified as CSF, above 130% (but below 192.5%) I_{WM}, classified as part of the GM mask; and under 130% (but over 50% to exclude air cavities) classified as WM, as shown in Figs. 3**b, c** and **d**. In-house software (MATLAB, The Mathworks Inc., Natick, MA), estimated each mask's volumes in every *j*-th voxel in the *k*-th subject (V_{jk}^{GM}, V_{jk}^{WM}, V_{jk}^{CSF}). The overall VOI, GM and WM tissue fractions (T_f, GM_f, WM_f) were obtained by dividing $V_{jk}^{(GM+WM)}$, V_{jk}^{GM}, V_{jk}^{WM} by the VOI volume.

Global GM and WM Concentrations

Since the CSF does not contribute to the ^{1}H-MRS signal, the *i*-th metabolite amount in the *j*-th voxel in the *k*-th subject can be modeled as the sum of two compartments' (GM, WM) amounts:

$$Q_{ijk}=Q_{ijk}^{GM}\cdot f_i^{GM}+Q_{ijk}^{WM}\cdot f_i^{WM}=C_{ik}^{GM}\cdot V_{jk}^{GM}\cdot f_i^{GM}+C_{ik}^{WM}\cdot V_{jk}^{WM}\cdot f_i^{WM}, \quad [4]$$

where C_{ik}^{GM}, C_{ik}^{WM} are the (unknown) global GM and WM metabolites' concentrations and the f_i-s are given by Eq. [2]. Since no significant GM and WM T_1^{vivo} differences are reported between 1.5 and 3 T (34), we used the values below Eq. [2]. For NAA, Cr, Cho and *m*I T_2^{vivo}*s* at 1.5 T we used 317, 208, 300 and 130 ms for the GM; and 361, 215, 330 and

110 ms for WM (34, 39). At 3 T, the T_2^{vivo}s used were 275, 157, 241 and 200 ms in GM; 400, 185, 258 and 200 ms in WM (32, 33). Although C_{ik}^{GM} and C_{ik}^{WM} cannot both be derived from Eq. [4], since the brain's GM and WM spatial heterogeneity is on a scale much smaller than the voxels, each has different, independent V_{jk}^{GM} and V_{jk}^{WM} coefficients. The resulting over-determined system of equations in C_{ik}^{GM} and C_{ik}^{WM} was solved with linear regression. The *inter*-subject coefficient of variation (CV=standard deviation/mean) of this approach has been shown to be under 15% (40).

Statistical Analysis

Due to the small sample size, there was not enough statistical power to formally test patient to control values for statistical significance. Therefore, a sample of 18 previously-studied healthy adults was used to derive 90% prediction intervals (40). Each metabolite concentration's (or tissue fraction's) mean, $\overline{X_i}$ and standard deviation, S_i, in the VOI and in its GM and WM moieties for a sample of N controls can be used to derive a 90% prediction interval for their value in a randomly-selected individual from the same population as,

$$\overline{X_i} \pm 1.65 \cdot \sqrt{1+1/N} \cdot S_i. \quad [5]$$

Consequently, if a new subject is observed to have a measured metric outside its prediction interval, either he or she is one of the 10% for whom this metric falls outside this interval, or, more likely, came from a population with a different distribution of values.

RESULTS

Our automatic shimming adjusted the whole-head water linewidth to 14 and 27 Hz at 1.5 and 3 T, yielding 12 and 22 Hz in the VOI without further adjustments. The VOI size and placement and ^{1}H spectra for the patients and controls, are shown in Figs. 1 and 2. The spectral fit quality is reflected by ‹20% mean Cramer-Rao lower bounds for all metabolites in the 1.0 cm^3 voxels' and ‹5.5% in the averaged VOI spectra, shown in Fig. 4. The global VOI and its GM and WM metabolite concentrations are compiled in Table 1. The NAA, Cr, Cho and *m*I concentrations 90% prediction intervals for the adults were obtained from their published values: 7.7±0.5, 5.4±0.5, 1.3±0.1 and 4.8±0.6 mM in the VOI; 7.6±0.5, 4.8±0.4, 1.4±0.2 and 4.6±0.7 mM in its WM; and 8.4±0.7, 6.7±0.6, 1.2±0.2 and 5.4±0.7 mM in the GM, using Eq. [5] (40).

The mean tissue fractions from the 18-subject sample were: 91±2%, 39±2% and 52±3% in VOI, GM and WM, and the resulting prediction intervals are also given in Table 1. In the adult patient, we observed 25% and 16% higher Cho in the VOI and its WM, respectively, and 17% lower NAA concentration in WM compared with controls' mean. All differences were outside their respective 90% prediction intervals (40). No metabolite was observed outside its 90% prediction interval for the adult control. For the children, no meaningful differences were observed between TSC patient and her control for any metabolite or tissue compartment, as shown in Table 1 and Fig. 4. Based on the reported similarity of pediatric spectra at this age to adults' (41, 42), we assume that because the differences between the patient and her control were relatively small (‹10% for any metabolite), the patient is within the 90% prediction interval of a representative healthy pediatric population.

Global VOI, GM and WM tissue fractions, T_f, GM_f. WM_f, are also shown in Table 1 for all subjects. For the adults, no tissue fraction was outside its relevant 90% prediction interval.

DISCUSSION

The low to modest correlation between brain tubers on clinical MRI and the neurologic phenotype of TSC strongly suggests that this modality does not define the full range of pathologic abnormalities. We therefore sought to use ^{1}H-MRS in MRI-negative TSC patients. The presence of MRS abnormalities in the adult TSC brain but not in the child is paradoxical since the child has developmental delay and refractory epilepsy, whereas the adult is neurologically normal. Several explanations may account for this double dissociation. First, the child did not have either *TSC1* or *TSC2* mutations on genetic testing although she met criteria for clinically-definite TSC (26). The cause for TSC in patients without *TSC1* or *2* mutations remains unknown, and may relate to either a third gene or regulatory DNA controlling *TSC1* or *2* (43). Thus, the pathophysiology of her disorder, although clinically parallel to patients with *TSC1*/*2* mutations, may result from another genetic disorder acting via a non-mTORC1 pathway. Second, the presence (or lack) of a *TSC1/2* mutation may be functionally dissociated from neurological symptoms; approximately 15% of children and adolescents with TSC have no CNS complications (43).

The MRS abnormalities in the adult, despite being neurologically asymptomatic, suggest that longer disease duration and/or *TSC2* gene mutation can cause: *(i)* axonal dysfunction, reflected by decreased WM NAA and elevated VOI and WM Cho suggesting demyelination that may lead to subsequent neuronal loss by Wallerian degeneration; and *(ii)* aberrant glial growth , reflected by elevated *m*I and Cr in the VOI and its GM (though not outside their 90% prediction intervals), possibly due to mTORC1 hyperactivity.

Several other neurologic processes could account for the dissociations between our pediatric and adult TSC subjects. Lack of abnormalities in the pediatric TSC brain may reflect ongoing development; *e.g.,* myelination may prevent or offset the demyelinating effects of hamartomas. Indeed, previous studies of the diffusion characteristics showed focal microstructural abnormalities limited to hamartomas, *i.e.*, no apparent diffusion coefficient differences in TSC patients versus controls in normal-appearing WM (44). In addition, cortical remodeling could also reverse or prevent changes to neurons and glia. Either mechanism, if substantiated, could have implications for therapy. Another possibility is that the underlying neuropathology in the child is in the 80–90% of the cortex outside the VOI (Fig. 1) missed in our study.

It is noteworthy that although not outside their 90% prediction intervals, GM_f was lower and WM_f was higher in both patients than their controls' (*cf.* Table 1). Although a curiosity, given the small *N*, and that TSC pathology is known to affect the cortex, it is perhaps not surprising that possible microscopic lesions and/or atrophy (that leaves healthy neurons intact) is responsible for both GM_f reductions. If deep GM nuclei within the VOI, *e.g.,* caudate, thalamus, *etc.,* shrink, the surrounding WM that would collapse inward to replace that lost volume may be responsible for the observed increased WM_f.

Admittedly, this study is also subject to several limitations: First, only two patients were enrolled, each belonging to a different age group and each representing a different genotype. However, given the rarity of MRI-negative TSC cases nationwide (about $1{:}10^5$), the Manhattan (2011 census population: 1.6 million (45)) area served by our epilepsy center would expect to see at most about sixteen. Since 10–20% of TSC patients do not experience seizures (43), they would not require an epilepsy center, the actual number of MRI-negative TSC patients available will usually underestimate the true prevalence; making two out of (at most) 16 a reasonable yield given our patient base (4). Second, each patient represented a subset not typically found in TSC. While these are rare conditions, their exploratory study is important for wider understanding of gene-function and/or its biomarker correlates. One

patient without *TSC1/2* mutation expresses a neurological phenotype while the other with the *TSC2* mutation had no neurological phenotype; this "double dissociation" points to the possible conclusion that mutation by itself has little bearing on neurologic outcome. It is noteworthy that approximately 15% of TSC patients have no CNS complications (43). Our MRS findings seem to support this functional dissociation. For instance, the asymptomatic adult showed lower WM NAA and higher WM Cho, which suggest neuro-axonal abnormalities associated with mutation, but not symptoms. Meanwhile similar MRS profiles between the children suggest that perhaps a different cause is needed to explain the patient's neurological symptoms. Either scenario, if substantiated, could have implications for treatment. Third, due to lipid contamination and signal "bleed" into surrounding voxels near/on lateral surfaces of the cerebral cortex, as well as poor shimming in those areas, our cortical coverage within the VOI was limited to cortex near the midline, *e.g.,* anterior and posterior cingulate.

Future studies with larger samples are needed to define the role of different genotypic features, *e.g.TSC1* versus *TSC2* versus non-*TSC1/2* specific mutations; and phenotypic features, *e.g.,* disease duration and severity, age, and specific clinical features such as intellectual disability, autism, epilepsy and their correlation with MRS abnormalities. Further investigation of the relationship of MRS abnormalities to neurologic phenotype in TSC could potentially provide diagnostic and prognostic information regarding brain development and function. It may also provide data relevant to defining epileptogenic versus nonepileptogenic brain tissue that could influence the identification and localization of seizure foci. Lastly, MRS could reveal new diagnostic biomarkers of mTORC1 brain dysfunction, which may help identify patients most likely to respond to mTOR inhibitors and monitor their response to therapy.

Acknowledgments

This work was supported by National Institutes of Health grants NS050520 and EB01015. Assaf Tal also acknowledges the support of the Human Frontiers Science Project.

REFERENCES

1. Osborne JP, Fryer A, Webb D. Epidemiology of tuberous sclerosis. Ann N Y Acad Sci. 1991; 615:125–127. Epub 1991/01/01. [PubMed: 2039137]
2. Dabora SL, Jozwiak S, Franz DN, Roberts PS, Nieto A, Chung J, et al. Mutational analysis in a cohort of 224 tuberous sclerosis patients indicates increased severity of TSC2, compared with TSC1, disease in multiple organs. Am J Hum Genet. 2001; 68(1):64–80. Epub 2000/12/12. [PubMed: 11112665]
3. Bourneville DM. Sclérose tubéreuse des circonvolutions cérébrales. Arch Neurol. 1880; 1:81–91.
4. Roach ES, Sparagana SP. Diagnosis of tuberous sclerosis complex. J Child Neurol. 2004; 19(9): 643–649. Epub 2004/11/26. [PubMed: 15563009]
5. Shepherd CW, Gomez MR. Mortality in the Mayo Clinic Tuberous Sclerosis Complex Study. Ann N Y Acad Sci. 1991; 615:375–377. Epub 1991/01/01. [PubMed: 2039164]
6. Jozwiak S, Schwartz RA, Janniger CK, Bielicka-Cymerman J. Usefulness of diagnostic criteria of tuberous sclerosis complex in pediatric patients. J Child Neurol. 2000; 15(10):652–659. Epub 2000/11/04. [PubMed: 11063078]
7. Curatolo P, Bombardieri R, Verdecchia M, Seri S. Intractable seizures in tuberous sclerosis complex: from molecular pathogenesis to the rationale for treatment. J Child Neurol. 2005; 20(4): 318–325. Epub 2005/06/01. [PubMed: 15921233]
8. Sparagana SP, Delgado MR, Batchelor LL, Roach ES. Seizure remission and antiepileptic drug discontinuation in children with tuberous sclerosis complex. Arch Neurol. 2003; 60(9):1286–1289. Epub 2003/09/17. [PubMed: 12975296]

9. Curatolo P, Cusmai R, Cortesi F, Chiron C, Jambaque I, Dulac O. Neuropsychiatric aspects of tuberous sclerosis. Ann N Y Acad Sci. 1991; 615:8–16. Epub 1991/01/01. [PubMed: 2039170]
10. Muzykewicz DA, Newberry P, Danforth N, Halpern EF, Thiele EA. Psychiatric comorbid conditions in a clinic population of 241 patients with tuberous sclerosis complex. Epilepsy Behav. 2007; 11(4):506–513. Epub 2007/10/16. [PubMed: 17936687]
11. Ridler K, Suckling J, Higgins N, Bolton P, Bullmore E. Standardized whole brain mapping of tubers and subependymal nodules in tuberous sclerosis complex. J Child Neurol. 2004; 19(9):658–665. Epub 2004/11/26. [PubMed: 15563011]
12. O'Callaghan FJ, Harris T, Joinson C, Bolton P, Noakes M, Presdee D, et al. The relation of infantile spasms, tubers, and intelligence in tuberous sclerosis complex. Arch Dis Child. 2004; 89(6):530–533. Epub 2004/05/25. [PubMed: 15155396]
13. Jansen FE, Vincken KL, Algra A, Anbeek P, Braams O, Nellist M, et al. Cognitive impairment in tuberous sclerosis complex is a multifactorial condition. Neurology. 2008; 70(12):916–923. Epub 2007/11/23. [PubMed: 18032744]
14. Madhavan D, Schaffer S, Yankovsky A, Arzimanoglou A, Renaldo F, Zaroff CM, et al. Surgical outcome in tuberous sclerosis complex: a multicenter survey. Epilepsia. 2007; 48(8):1625–1628. Epub 2007/05/09. [PubMed: 17484758]
15. Wong M. The utility of tuberless models of tuberous sclerosis. Epilepsia. 2007; 48(8):1629–1630. author reply 32–4. Epub 2007/08/19. [PubMed: 17692051]
16. Wang Y, Greenwood JS, Calcagnotto ME, Kirsch HE, Barbaro NM, Baraban SC. Neocortical hyperexcitability in a human case of tuberous sclerosis complex and mice lacking neuronal expression of TSC1. Ann Neurol. 2007; 61(2):139–152. Epub 2007/02/07. [PubMed: 17279540]
17. Meikle L, Talos DM, Onda H, Pollizzi K, Rotenberg A, Sahin M, et al. A mouse model of tuberous sclerosis: neuronal loss of Tsc1 causes dysplastic and ectopic neurons, reduced myelination, seizure activity, and limited survival. J Neurosci. 2007; 27(21):5546–5558. Epub 2007/05/25. [PubMed: 17522300]
18. Griffiths PD, Hoggard N. Distribution and conspicuity of intracranial abnormalities on MR imaging in adults with tuberous sclerosis complex: A comparison of sequences including ultrafast T2-weighted images. Epilepsia. 2009; 50(12):2605–2610. Epub 2009/06/06. [PubMed: 19490046]
19. Luat AF, Makki M, Chugani HT. Neuroimaging in tuberous sclerosis complex. Curr Opin Neurol. 2007; 20(2):142–150. Epub 2007/03/14. [PubMed: 17351483]
20. Marcotte L, Aronica E, Baybis M, Crino PB. Cytoarchitectural alterations are widespread in cerebral cortex in tuberous sclerosis complex. Acta Neuropathol. 2012; 123(5):685–693. Epub 2012/02/14. [PubMed: 22327361]
21. Magri L, Cambiaghi M, Cominelli M, Alfaro-Cervello C, Cursi M, Pala M, et al. Sustained activation of mTOR pathway in embryonic neural stem cells leads to development of tuberous sclerosis complex-associated lesions. Cell Stem Cell. 2011; 9(5):447–462. Epub 2011/11/08. [PubMed: 22056141]
22. Benarroch EE. N-acetylaspartate and N-acetylaspartylglutamate: neurobiology and clinical significance. Neurology. 2008; 70(16):1353–1357. Epub 2008/04/17. [PubMed: 18413589]
23. Soares DP, Law M. Magnetic resonance spectroscopy of the brain: review of metabolites and clinical applications. Clinical radiology. 2009; 64(1):12–21. [PubMed: 19070693]
24. Mountford CE, Stanwell P, Lin A, Ramadan S, Ross B. Neurospectroscopy: the past, present and future. Chem Rev. 2010; 110(5):3060–3086. Epub 2010/04/15. [PubMed: 20387805]
25. Ross B, Bluml S. Magnetic resonance spectroscopy of the human brain. Anat Rec. 2001; 265(2): 54–84. Epub 2001/04/27. [PubMed: 11323770]
26. Roach ES, Gomez MR, Northrup H. Tuberous sclerosis complex consensus conference: revised clinical diagnostic criteria. J Child Neurol. 1998; 13(12):624–628. Epub 1999/01/09. [PubMed: 9881533]
27. Hu J, Javaid T, Arias-Mendoza F, Liu Z, McNamara R, Brown TR. A fast, reliable, automatic shimming procedure using 1H chemical-shift-imaging spectroscopy. J Magn Reson B. 1995; 108(3):213–219. [PubMed: 7670755]

28. Goelman G, Liu S, Hess D, Gonen O. Optimizing the efficiency of high-field multivoxel spectroscopic imaging by multiplexing in space and time. Magn Reson Med. 2006; 56(1):34–40. [PubMed: 16767711]
29. Gonen O, Murdoch JB, Stoyanova R, Goelman G. 3D multivoxel proton spectroscopy of human brain using a hybrid of 8th-order Hadamard encoding with 2D chemical shift imaging. Magn Reson Med. 1998; 39(1):34–40. [PubMed: 9438435]
30. Soher BJ, Young K, Govindaraju V, Maudsley AA. Automated spectral analysis III: application to in vivo proton MR spectroscopy and spectroscopic imaging. Magn Reson Med. 1998; 40(6):822–831. [PubMed: 9840826]
31. Ethofer T, Mader I, Seeger U, Helms G, Erb M, Grodd W, et al. Comparison of longitudinal metabolite relaxation times in different regions of the human brain at 1.5 and 3 Tesla. Magn Reson Med. 2003; 50(6):1296–1301. [PubMed: 14648578]
32. Kirov II, Fleysher L, Fleysher R, Patil V, Liu S, Gonen O. Age dependence of regional proton metabolites T2 relaxation times in the human brain at 3 T. Magn Reson Med. 2008; 60(4):790–795. Epub 2008/09/26. [PubMed: 18816831]
33. Posse S, Otazo R, Caprihan A, Bustillo J, Chen H, Henry PG, et al. Proton echo-planar spectroscopic imaging of J-coupled resonances in human brain at 3 and 4 Tesla. Magn Reson Med. 2007; 58(2):236–244. Epub 2007/07/05. [PubMed: 17610279]
34. Traber F, Block W, Lamerichs R, Gieseke J, Schild HH. 1H metabolite relaxation times at 3.0 tesla: Measurements of T1 and T2 values in normal brain and determination of regional differences in transverse relaxation. J Magn Reson Imaging. 2004; 19(5):537–545. [PubMed: 15112302]
35. Kreis R, Slotboom J, Hofmann L, Boesch C. Integrated data acquisition and processing to determine metabolite contents, relaxation times, and macromolecule baseline in single examinations of individual subjects. Magn Reson Med. 2005; 54(4):761–768. Epub 2005/09/15. [PubMed: 16161114]
36. Kirov II, George IC, Jayawickrama N, Babb JS, Perry NN, Gonen O. Longitudinal interand intra-individual human brain metabolic quantification over 3 years with proton MR spectroscopy at 3 T. Magn Reson Med. 2012; 67(1):27–33. Epub 2011/06/10. [PubMed: 21656555]
37. Mikheev A, Nevsky G, Govindan S, Grossman R, Rusinek H. Fully automatic segmentation of the brain from T1-weighted MRI using Bridge Burner algorithm. J Magn Reson Imaging. 2008; 27(6): 1235–1241. Epub 2008/05/28. [PubMed: 18504741]
38. Sled JG, Zijdenbos AP, Evans AC. A nonparametric method for automatic correction of intensity nonuniformity in MRI data. IEEE Trans Med Imaging. 1998; 17(1):87–97. Epub 1998/06/09. [PubMed: 9617910]
39. Frahm J, Bruhn H, Gyngell ML, Merboldt KD, Hanicke W, Sauter R. Localized proton NMR spectroscopy in different regions of the human brain in vivo. Relaxation times and concentrations of cerebral metabolites. Magn Reson Med. 1989; 11(1):47–63. Epub 1989/07/01. [PubMed: 2747516]
40. Tal A, Kirov II, Grossman RI, Gonen O. The role of gray and white matter segmentation in quantitative proton MR spectroscopic imaging. NMR Biomed. 2012 Epub 2012/06/21.
41. Bluml S, Wisnowski JL, Nelson MD Jr, Paquette L, Gilles FH, Kinney HC, et al. Metabolic Maturation of the Human Brain From Birth Through Adolescence: Insights From In Vivo Magnetic Resonance Spectroscopy. Cereb Cortex. Epub 2012/09/07.
42. Kreis R, Ernst T, Ross BD. Development of the human brain: in vivo quantification of metabolite and water content with proton magnetic resonance spectroscopy. Magn Reson Med. 1993; 30(4): 424–437. [PubMed: 8255190]
43. Curatolo P, Bombardieri R, Jozwiak S. Tuberous sclerosis. Lancet. 2008; 372(9639):657–668. Epub 2008/08/30. [PubMed: 18722871]
44. Firat AK, Karakas HM, Erdem G, Yakinci C, Bicak U. Diffusion weighted MR findings of brain involvement in tuberous sclerosis. Diagnostic and interventional radiology. 2006; 12(2):57–60. Epub 2006/06/06. [PubMed: 16752348]
45. New York County QuickFacts from the U.S. Census Bureau. United States Census Bureau. 2011. Available from: http://quickfacts.census.gov/qfd/states/36/36061.html.

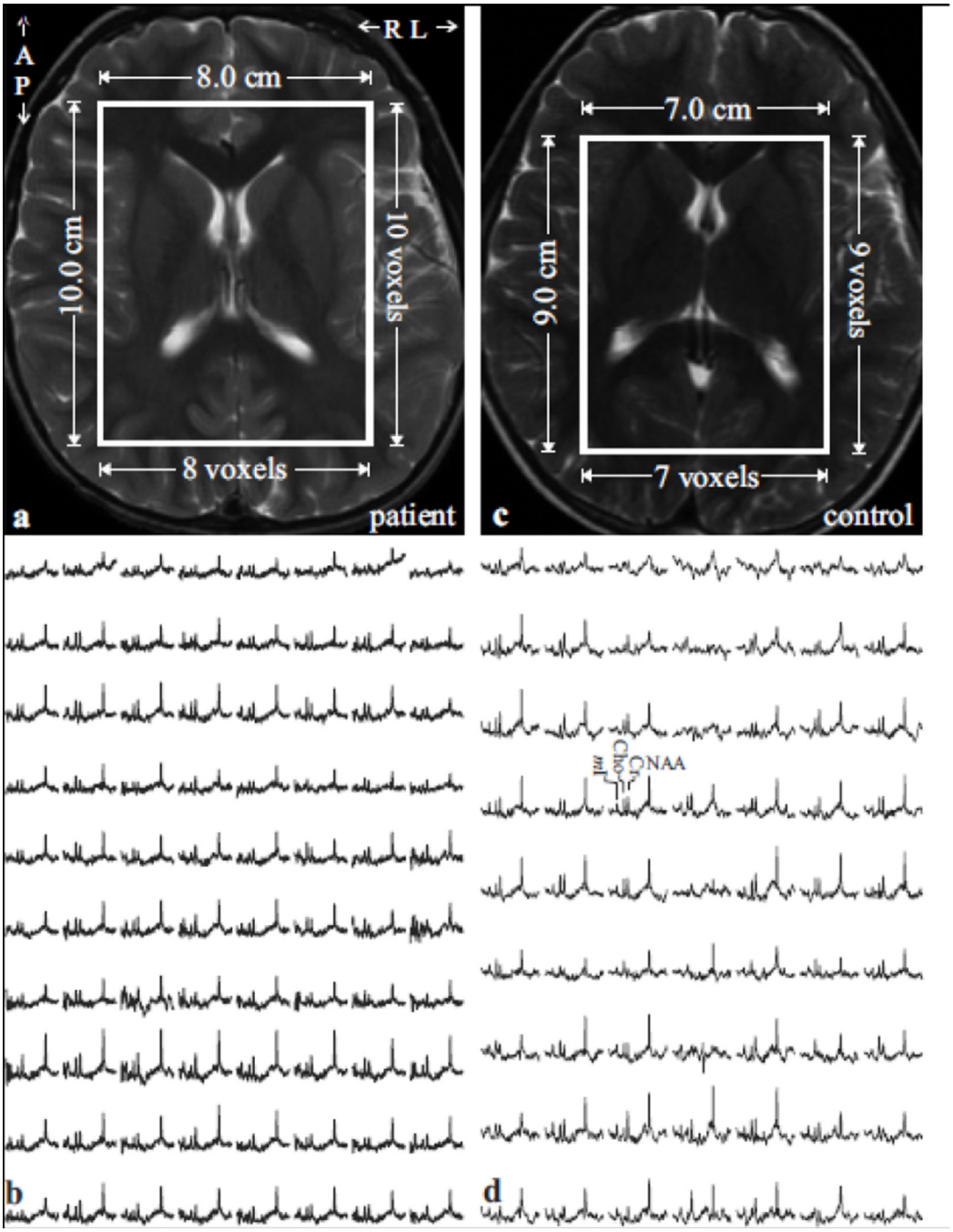

Fig. 1.

Top left, (**a**): Axial T_2-weighted TSE MRI of a 5-year old female TSC patient brain shows the location and size of the VOI (solid white frame). Note the absence of tubers.

Bottom left, (**b**): Real part of the 8×10 (LR×AP) ^{1}H spectra matrix from the VOI in **a**, on common chemical shift and intensity scales. Note the spectra resolution and SNR from these 1.0 cm^3 voxels in ~35 minutes of 3D ^{1}H-MRS acquisition at 1.5 T.

Top/Bottom right: (**c, d**): Same as (**a, b**), except for an age- and gender-matched control.

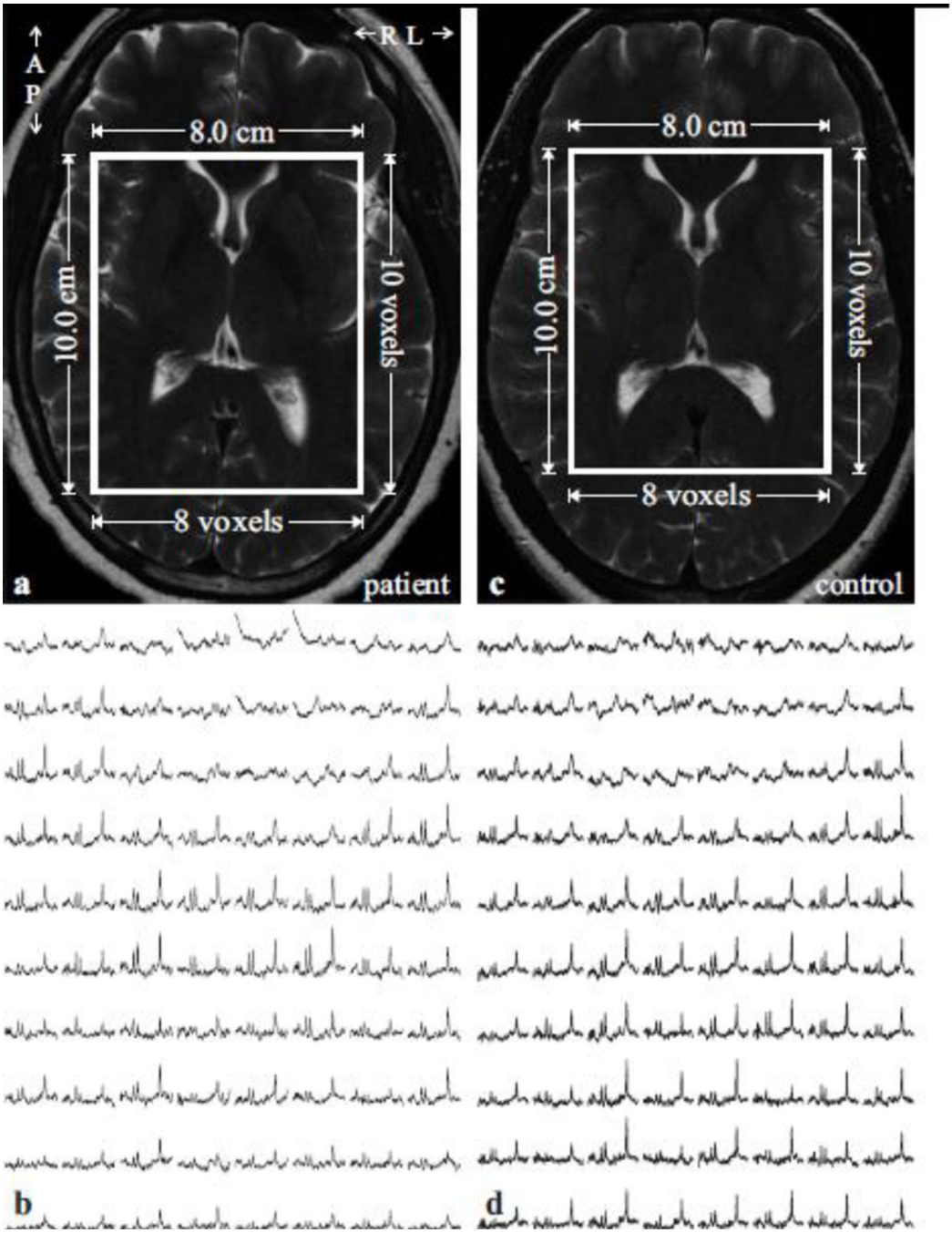

Fig. 2.

Top left, (**a**): Axial T_2-weighted TSE MRI of a 43-year old female TSC patient brain shows the location and size of the VOI (solid white frame). Note the absence of tubers.

Bottom left, (**b**): Real part of the 8×10 (LR×AP) ^{1}H spectra matrix from the VOI in **a**, on common chemical shift and intensity scales. Note the spectra resolution and SNR of the 0.75 cm^3 voxels in ~30 minutes of 3D ^{1}H-MRS acquisition at 3 T.

Top/Bottom right: (**c, d**): Same as (**a, b**), except for an age- and gender-matched control.

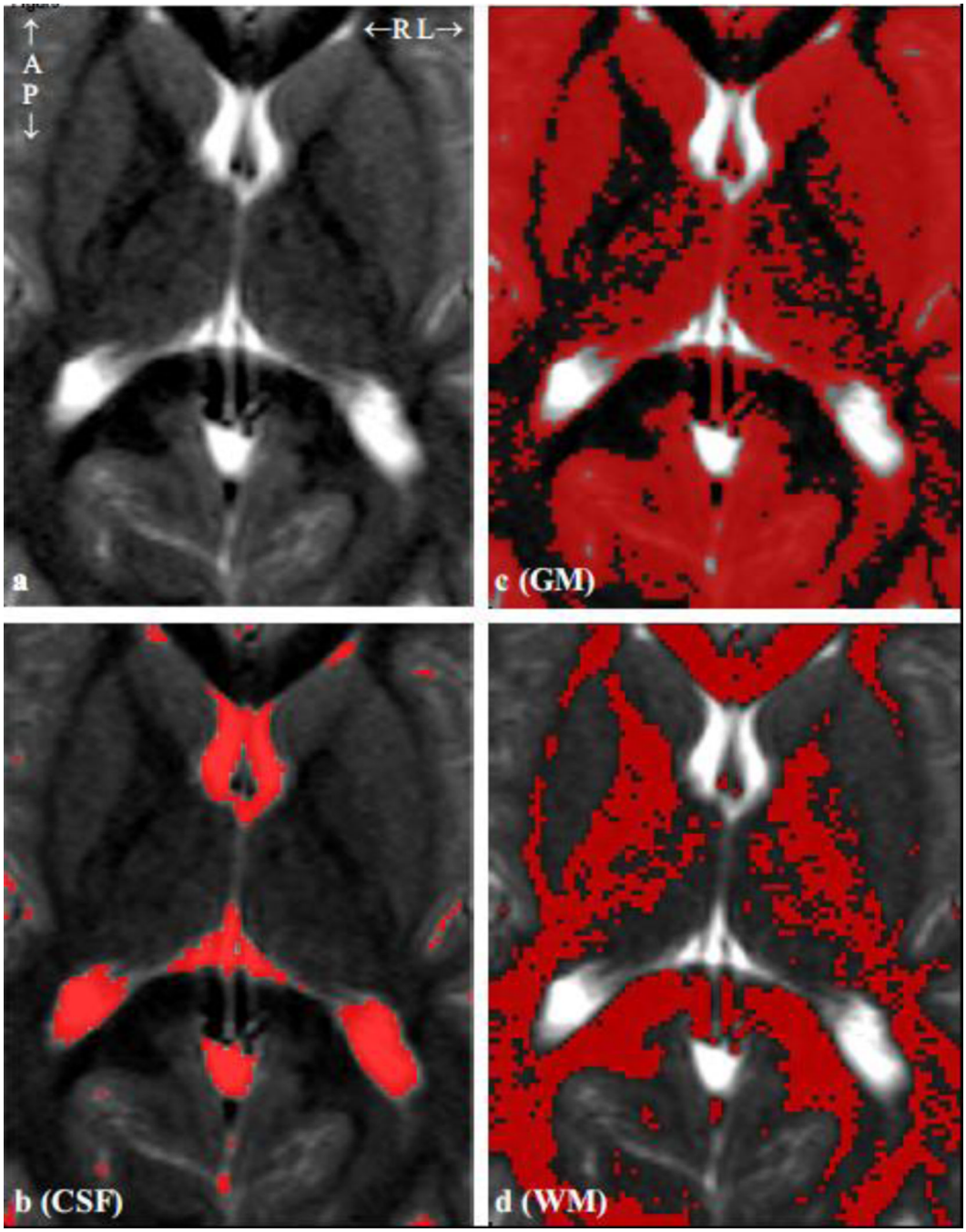

Fig. 3.

a: Axial T_2-weighted TSE MRI of a healthy 6-year old brain showing the 7×9 cm^2 VOI. **b – d**: same as **a**, overlaid with FireVoxel generated CSF, GM and WM masks used to obtain their VOI fractions for Eqs. [3] and [4]. Note the tissue segmentation accuracy.

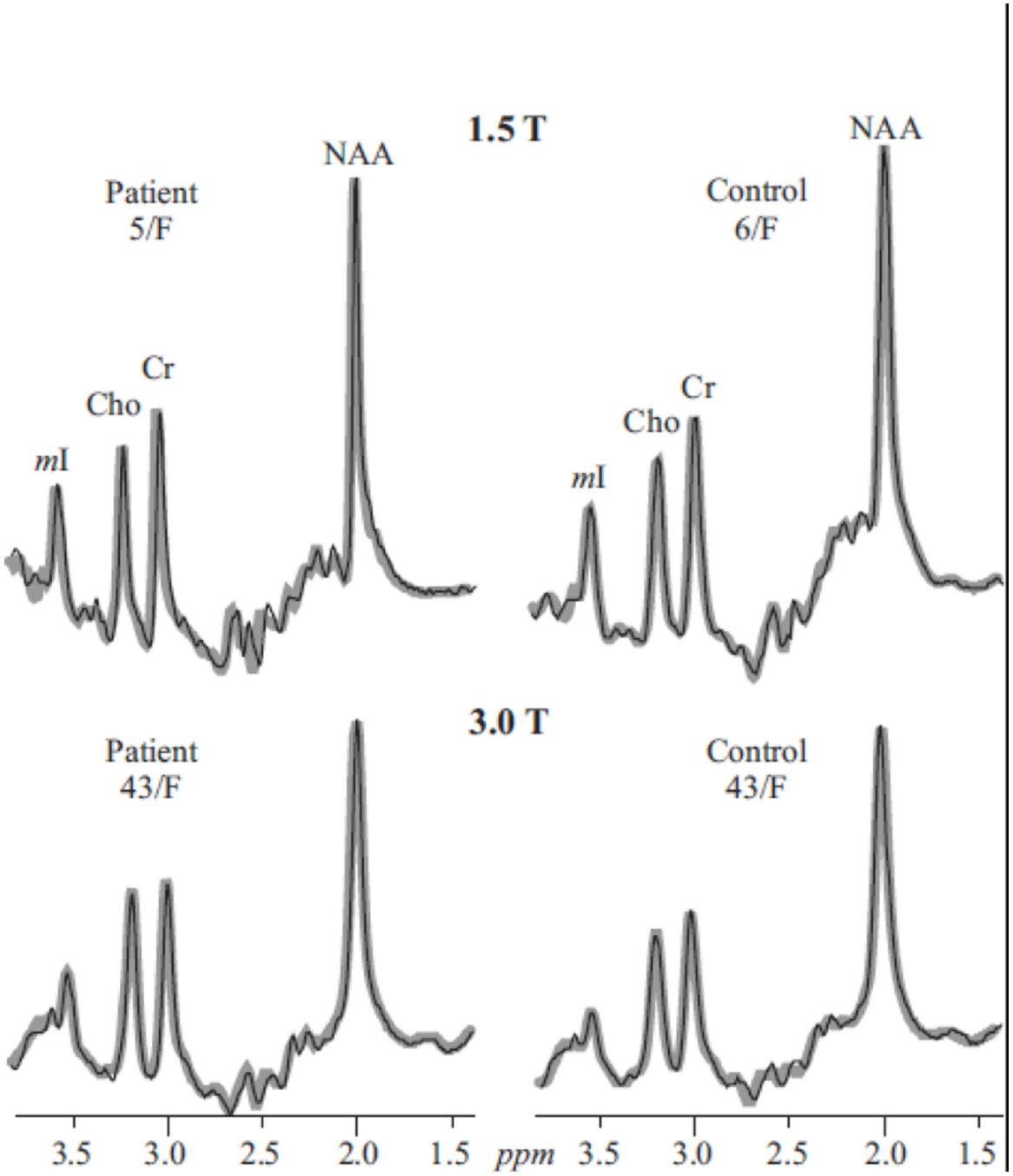

Fig. 4.

Real part of the aligned and globally-averaged ^{1}H spectra from all VOI voxels (thin black lines) representing Eq. [3], for each subject, superimposed with their fitted model functions (thick gray lines), on common intensity (at each field) and chemical shift scales. Note the excellent SNRs and resolution (compared with the single voxels in Figs. 1 and 2) and observable Cho, Cr and *m*I increases in the adults (See Table 1).

TABLE 1

Absolute metabolite concentrations and tissue fraction for each region for both TSC patients and their matched controls.

Region	Metabolite[a]	[a]Pediatric		[a]Adult	
		TSC	[b]Control	TSC	[b]Control
VOI	NAA	9.7	9.8	7.4	7.8 [6.8, 8.6]
	Cr	6.2	63	6.1	5.8 [4.7, 6.2]
	Cho	1.4	1.4	**1.6**	1.3 [1.1, 1.5]
	*m*I	6.0	5.7	5.2	4.3 [3.8,5.8]
[c]T_f		91	89	92	91 [90, 99]
GM	NAA	12.5	12.5	8.8	8.0 [7.2, 9.6]
	Cr	8.3	9.0	7.4	6.9 [5.7, 7.8]
	Cho	1.6	1.6	1.4	1.3 [0.9, 1.5]
	*m*I	7.9	7.3	6.2	4.7 [4.2, 6.5]
[c]GM_f		41	44	38	42 [36, 43]
WM	NAA	8.5	8.4	**6.3**	7.7 [6.8, 8.5]
	Cr	5.0	4.6	4.9	4.8 [4.1,5.6]
	Cho	1.5	1.4	**1.6**	1.4 [1.1, 1.6]
	*m*I	5.0	4.6	4.4	4.3 [3.4, 5.7]
[c]WM_f		51	45	53	49 [47, 57]

[a]millimoles/kg wet weight

[b][lower bound, upper bound] is the 90% prediction interval (Eq. [5]) for each metabolite/tissue fraction derived from a sample of 18 healthy adults (40).

[c]Percent (%). **Bold** type indicates a value outside its 90% prediction interval.